# WBAN Channel Modeling for 900 MHz and 60 GHz Communications

Reza Aminzadeh, Arno Thielens, *Member, IEEE,* Maxim Zhadobov, *Senior Member, IEEE,* Luc Martens, *Member, IEEE,* and Wout Joseph, *Senior Member, IEEE*

***Abstract*—This paper deals with the experimental characterization of the on-body propagation channel for applications in wireless body area networks (WBAN)s. The on-body propagation was studied between two quarter-wavelength monopole antennas in the 900 MHz band and between two horn antennas in the 55-65 GHz range. Different locations all over the body, including arm, leg, front and back of the torso were studied for two human male subjects. The channel parameters in terms of path gain and delay spread were extracted from measurements for vertical and horizontal polarizations of the antennas in both frequency bands. Additionally, a wrist to arm path was studied in the 60 GHz band where the transmitter was rotated in 360° around the arm at a fixed distance from the receiver. We obtained a path gain exponent between 2 and 3 in the 900 MHz band and in the 2.4 to 6 range for the 60 GHz band. Higher path gains for vertical and horizontal polarizations were obtained in the 900 MHz and 60 GHz bands, respectively. Maximum mean excess delay and root mean square delay spread were 6.3 ns and <2 ns in the 900 MHz band, respectively, while these values decreased by factors 3 and 10 in the 60 GHz band.**

***Index Terms*—Wireless body area network, on-body propagation, path gain, millimeter waves, delay spread.**

## I. Introduction

WIRELESS body area networks (WBANs) are becoming increasingly important. These body-worn networks of wireless nodes are expected to enable many wearable applications including medical [1], [2]. The current studies on WBANs mainly focus on frequencies below 6 GHz [1], [3]–[5]. The first generation of studies on-body channels focused on specific communication scenarios, such as for example wrist-to-head communication [6], [7], while later studies on WBANs focused on channel modeling [8], [9]. This led to the development of a standard (IEEE 802.15.6) for wireless, radio-frequency (RF) communication in WBANs [3]. Industrial, Scientific, and Medical (ISM) frequency bands around 900 MHz have been studied specifically for WBANs in [3], [5], [7], [10], [11]. These frequency bands have the advantage of license-free operation and the possibility to use the ultra-high-frequency radio-frequency identification (UHF-RFID) standard for back-scatter communication [5], [7], [12].

It is expected that the number of nodes in a WBAN will increase and that the requirements put forward by those nodes on the WBAN will be more stringent [13]. Certain nodes, such as brain-machine interfaces or smart prostheses, will require very high data rates and very low latency. Additionally, there is a need for more wearability of the nodes in the WBAN, which could be achieved by working with smaller antennas. A possibility to provide both higher band widths and smaller antenna footprints is to communicate at relatively high RF frequencies. A potential frequency band for WBANs would be the license-free band around 60 GHz.

In order to assess the potential of higher microwave frequencies, such as 60 GHz, a channel model needs to be built. Previous studies have dealt with on-body antennas at 60 GHz [14]–[16] and have used such antennas for on-body channel loss measurements [14], [17], [18]. However, these reports either focus on a theoretical analysis [17] or measure channel loss in specific situations such as head-to-shoulder, wrist-to-trunk and wrist-to-chest [14] as well as belt-to-head [18]. They neither provided a channel model at 60 GHz nor studied extensively various locations on the body. Additionally, the aforementioned studies do not benchmark the channel at 60 GHz with the competing channels at lower frequencies, which makes it difficult to compare those options for communication in WBANs. An attempt at such a comparison is done by [19], but this is only executed in a single on-body configuration, while previous studies have already demonstrated that large differences in the on-body channel can occur between different on-body configurations [5].

The main goal of this study is to design and compare on-body channel model at 900 MHz and 60 GHz. To this aim, on-body channel loss measurements are performed 1) on two human subjects; 2) in five scenarios; 3) in the two frequency bands: 900 MHz and around 60 GHz (at 55, 60 and 65 GHz); 4) for two parallel polarizations of antennas and 5) for a wrist to arm scenario including rotation of transmitting antenna in the 60 GHz band. These measurements are fed into a channel loss model and compared for both frequencies.

## II. Propagation mechanisms

The body channel communication at the studied frequencies in this manuscript is usually characterized by wave propagation [20], [21]. The capacitive coupling method is used below tens of MHz. Propagation of vertically (V) and horizontally (H) polarized electromagnetic fields on a flat conductive surface was described in [22], [23] and at 60 GHz in [17]. For a V-polarized wave, the electric field $E_r$ at the location of a receiver at a height of $h_r$ and distance $d$ from a transmitter

This work was supported by the Research Foundation Flanders (FWO) under grant agreement No G003415N.

R. Aminzadeh, A. Thielens, L. Martens and W. Joseph are with the Waves Research group, Department of Information Technology, Ghent University/imec, B-9052 Ghent, Belgium (e-mail: reza.aminzadeh@ugent.be).

M. Zhadobov is with the Institute of Electronics and Telecommunications of Rennes (IETR), UMR CNRS 6164, University of Rennes 1, 35042 Rennes.

at height $h_t$, can be expressed (near the surface) as [17], [22], [23]:

$$E_r = E_{QS} + E_{geom} + E_{surf} \quad (1)$$

with $E_r$ the electric field at the receiver, $E_{QS}$ is the quasi-static field, $E_{geom}$ is the geometrical-optics field, and $E_{surf}$ is the Norton Surface wave. The relative amplitudes of these terms depend on $d$, $h_r$, $h_t$, the dielectric parameters of the conductive surface, and the transmitter and receiver parameters. Expressions for all terms can be found in [17], [22], [23]. The validity of this approximation is discussed in [17] and requires that $h_t$ and $h_r$ are small in comparison to the wavelength. The first term in Eq. 1 governs the near-field transmission (quasi-static coupling) and has a $1/d^3$ dependency. At 60 GHz, this component is small at propagation distances of several centimeters [17]. The second and third terms will be dominant in the channel measurements executed in this study (see Section III). Both terms have a $1/d^2$ dependency [17], which has led to the proposal of the following channel gain/loss model in [17]:

$$G(d,f) = G(d_0,f) - 10.n(f).log_{10}(\frac{d_f}{d_{0,f}}) + X_\sigma(f) \quad (2)$$

with $f$, the frequency, $G(d,f)$ the channel gain in decibels, $d_{0,f}$ an arbitrary reference distance, $n(f)$ the channel gain exponent, and $X_\sigma(f)$ the log-normal variance on the path gain. In free space $n$ equals 2. As [17] proposes a $1/d^2$ dependency of the surface waves, they predicted and found an $n = 4$ for the channel loss, which is a power that scales with $E_r^2$ [17]. Although, eq. 2 is frequency-dependent, for the sake of simplicity $f$ is not mentioned for the above-mentioned parameters in the rest of the paper.

Another analysis can be done for H-polarized waves, leading to a similar channel gain model [17]. Therefore, this model (eq. 2) will be used in Section III to process the measurement data.

## III. Methodology

This section presents the methodology used in the on-body channel gain measurements. First, the measurement configuration is outlined. Second, the used antennas and RF equipment are described. Third, the channel modeling is described.

### A. On-Body Measurements Configuration

The goal of the on-body measurements is to model the on-body channel gain between a transmitter (Tx) and a receiver (Rx) as a function of distance along different body parts: front and back of the torso, arms, and legs, respectively, for multiple subjects. Two human male subjects were recruited for this study and are denoted as subject under test, SUT-1 and 2 with heights and body masses of 169 cm and 75 kg, and 172 cm and 58 kg, respectively. Laser beams were used to achieve straight lines on the body regardless of the curved surfaces on the body. Additionally, for each subject, we measured the distance of each measurement line to different body parts to ensure that the measurements were performed on the same spot. The measurements are performed in two frequency bands: around 900 MHz and around 60 GHz.

*1) 900 MHz Frequency Band:* Fig. 1(a) shows the on-body configuration for measurements at 900 MHz. Two identical monopole antennas are considered as the Tx and Rx and are placed on ground planes of $\lambda/4$ (8.3 cm). The center of the feed connector of each monopole antenna was used as an indicator to ensure that the measurements were repeated at the same location. The antennas have a reflection coefficient lower than -10 dB (on body) at the desired frequency (900 MHz here). Two configurations of the antennas are considered: H-polarization, i.e. polarization parallel to the skin, denoted as HH, and V-polarization, i.e. polarization orthogonal to the skin, denoted as VV. The antennas were placed at a minimum distance of 10 cm and at a height of 0.5 cm from the body [4], [9]. We always placed the monopole orthogonally to the body's surface (V-polarization) or parallel to the surface (H-polarization). We neither aimed at investigating a fixed antenna orientation w.r.t the body. We did nor strive towards a maximal gain in every measurement configuration. In total 252 measurements were performed along the right arm, right leg, front and back of the torso. The Tx was always fixed while the Rx moved away from the Tx in steps of 7.5 cm up to a separation distance of 50 cm. Additionally, a non-line-of-sight (NLOS) scenario is considered from front torso to the back (via left shoulder) up to a separation distance of 50 cm.

*2) 60 GHz Frequency Band:* Fig. 1(b) shows the on-body configuration for measurements in the 55-65 GHz range. Two identical horn antennas (QMS-00475, Steatite Antennas, UK) are considered as the Tx and Rx. The center of the feed connector of each horn antenna was placed on the indicated spots on the body (see Fig. 1(b)) to ensure measurement of the maximum gain. The antennas have a reflection coefficient lower than -10 dB (on body) in the target frequency band (55-65 GHz here). Two co-polarized configurations (HH and VV) of the antennas are considered. The antennas were placed at a minimum distance of 5 cm and at a height of 0.5 cm from the body. In total 316 measurements were performed along the right arm, right leg, front and back of the torso. The Tx (stars) was always fixed while the Rx (circles) moved away from the Tx in steps of 3 cm up to a separation distance of 50 cm.

*3) Wrist to arm scenario in the 60 GHz frequency band:* A potential rotation of the TX around the wrist is studied. Figure 2(a) depicts the proposed measurement scenario and the measurement setup is shown in Fig. 2(b). Similar to Section III-A2, for both subjects the Tx was placed on 360° and was rotated over the wrist in approximate steps of 45°. The Rx was fixed during the measurements at a separation distance of 10 cm. The goal of this measurement is to study the channel gain for rotated Tx on the wrist. Both V- and H-polarizations of Tx-Rx were considered in this setup.

### B. Measurement Setup

First, for both 900 MHz (see Fig. 1(c)) and 60 GHz (Fig. 1(d)) frequency bands, the Tx and Rx were connected to a Vector Network Analyzer (ZVA 67, Rohde & Schwarz), which swept over a frequency band from 700 MHz-4 GHz and 55-65 GHz in 1024 equidistant frequency steps. 20 sweeps of all

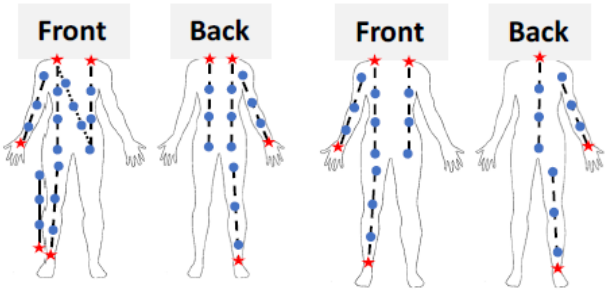


(a) 900 MHz (b) 55-65 GHz

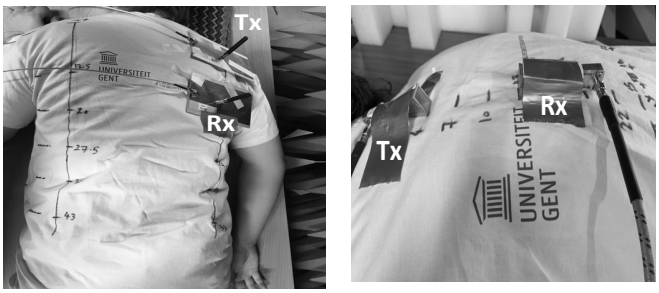


(c) 900 MHz (d) 55-65 GHz

Fig. 1. The proposed on-body configuration (a-b) and the measurement setup (c-d) for the studied frequency bands: (a-b) Tx and Rx are indicated by stars and circles, respectively; the solid line indicates measurements on the outer side of the leg; dotted line on the chest shows the measurements performed diagonally on the front torso. (c) Measurements on the back of torso with two vertically polarized antennas at 900 MHz. (d) Measurements on the back of torso with two horn antennas with horizontal polarizations in the 55-65 GHz range. The Tx and Rx are indicated by stars and circles, respectively.

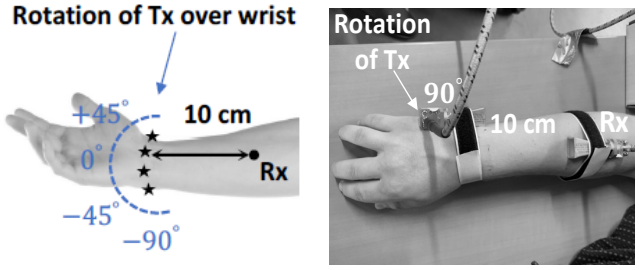


(a) (b)

Fig. 2. (a) The proposed configuration of Tx-Rx for wrist to arm channel gain measurements in the 55-65 GHz range. (b) VV-configuration of two horn antennas on an arm with Tx rotated 90° relative to Rx at a separation distance of 10 cm.

two-port S parameters were registered for every measurement configuration and averaged for processing. The $S_{21}$ and $S_{12}$ parameters obtained from the on-body measurements in different on-body scenarios and different frequency bands were used as an input to the channel gain model described by Eq. 2 and used for a maximum likely estimation of the parameters ($G_0$, $n$) with $d_0$ the minimal separation distance.

The authors of [24] pointed that using measurement equipment such as those we used in this paper could create extra channels (e.g. induced and un-balanced current flows in the cables, VNA, etc.) that may potentially undermine the validity of the measured data. The length of the cables used in our study is 1 m. Six high frequency ferrite clamps were placed at equal distances along each cable during the measurements to suppress differential or common-mode conducted electromagnetic interference. Additionally, to ensure that the effect of additional channels is negligible in our measurements, we performed path gain measurements (VV monopole antennas at 900 MHz on the leg of a male subject) with two cables of different length i.e. 1 m and 2 m. We observed that increasing the length of the cable from 1 m to 2 m caused an average deviation of 0.8 dB and a maximum deviation of 1.5 dB on the measured path gain at each measured distance on the body.

### C. Wrist to arm channel model: 60 GHz frequency band

The channel gains were measured at several Tx-Rx separation distances along the arm (see Section III-A2) and for rotation of Tx around the wrist with the Rx placed on the arm at a fixed location and distance of 10 cm from the Tx (see Section III-A3). The initial positioning is usually performed with perfect alignment of Tx-Rx polarizations while the rotation introduces polarization mismatch between Tx-Rx when Tx is rotated. Additionally, in case of rotated Tx, the field will propagate along a curved surface instead of an approximately straight path. The polarization mismatch between two linearly polarized antennas is expressed as follows [25]:

$$g(\psi) = g(0^\circ).cos^2(\psi) \tag{3}$$

where $g$ is the linear channel gain and $\psi$ is the angle between the polarizations of the Tx and Rx. When either the Tx or the Rx is rotated, the channel gain decreases for $0^\circ < \psi < 90^\circ$ and increases again for $90^\circ < \psi < 180^\circ$. In [10], it was shown that the channel gain along a curved surface decays exponentially with distance:

$$G(d) = G(d_0) + 10.log_{10}(e^{-\alpha d}) + X_\sigma \tag{4}$$

with $G(d)$ the channel gain in decibels, $d_0$ an arbitrary reference distance, $\alpha$ the loss per unit distance, and $X_\sigma$ the log-normal variance on the path gain. It is clear that when either Tx or Rx is rotated, $d$ changes as a function of $\psi$. Both equations (3) and (4) predict a decrease in channel gain for $0^\circ < \psi < 90^\circ$. Here we fit a two-slope model similar to the one proposed in [11] for propagation around human body:

$$G(\theta) = \begin{cases} G(0^\circ) - \alpha_1.|\theta| & \text{for } \theta \in [-\theta_c, +\theta_c], \\ G(\theta_c) - \alpha_2.(|\theta| - \theta_c) & \text{for } \theta \in [-\pi, -\theta_c] \ \ \& \ \ [\theta_c, \pi]. \end{cases} \tag{5}$$

where $\theta$ and $\theta_c$ are the angle of rotation around the arm and the transition angle (or breakpoint), respectively. $\alpha_1$ and $\alpha_2$ are the two losses over distance (unit: $dB/^\circ$) with $\alpha_1 > \alpha_2$.

### D. Delay spread

The mean excess delay ($\tau_0$) and the root mean square (RMS) delay spread ($\tau_{rms}$) are calculated from the first moment and square root of the second central moment of the power delay profile (PDP). First, for every studied path on body, the PDP is calculated from the squared magnitude of the channel impulse response for that path. Second, a threshold of 6 dB above the

This article has been accepted for publication in a future issue of this journal, but has not been fully edited. Content may change prior to final publication. Citation information: DOI 10.1109/TAP.2020.3045498, IEEE Transactions on Antennas and Propagation



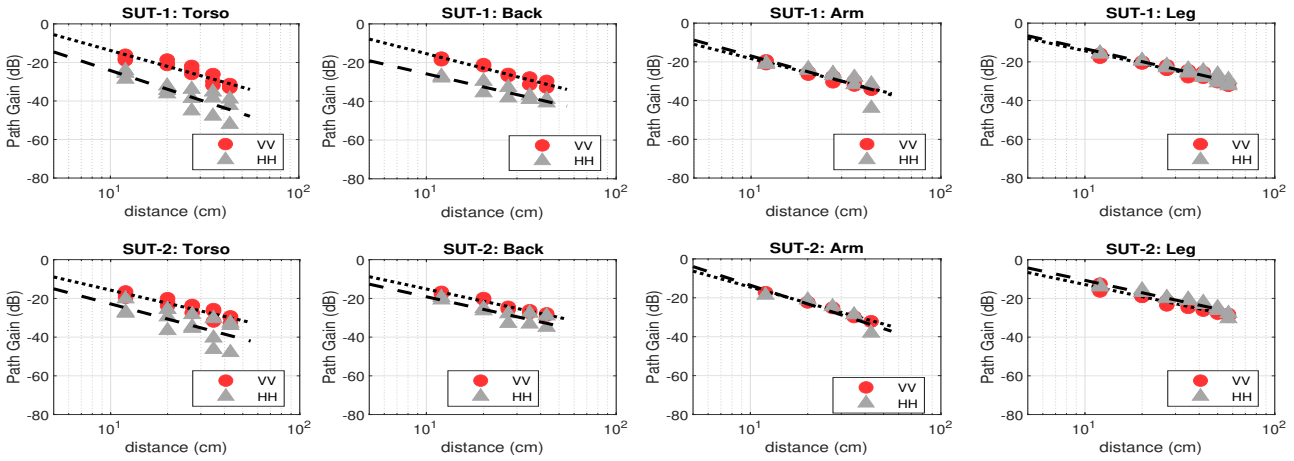


Fig. 3. Comparison of the modeled path gains for different polarizations of Tx-Rx antennas on body (VV vs. HH) for two subjects along the arm, leg, front and back of the torso at 900 MHz. Measurements-VV: circles; measurements-HH: triangles; fit-VV: dotted line; fit-HH= dashed line.

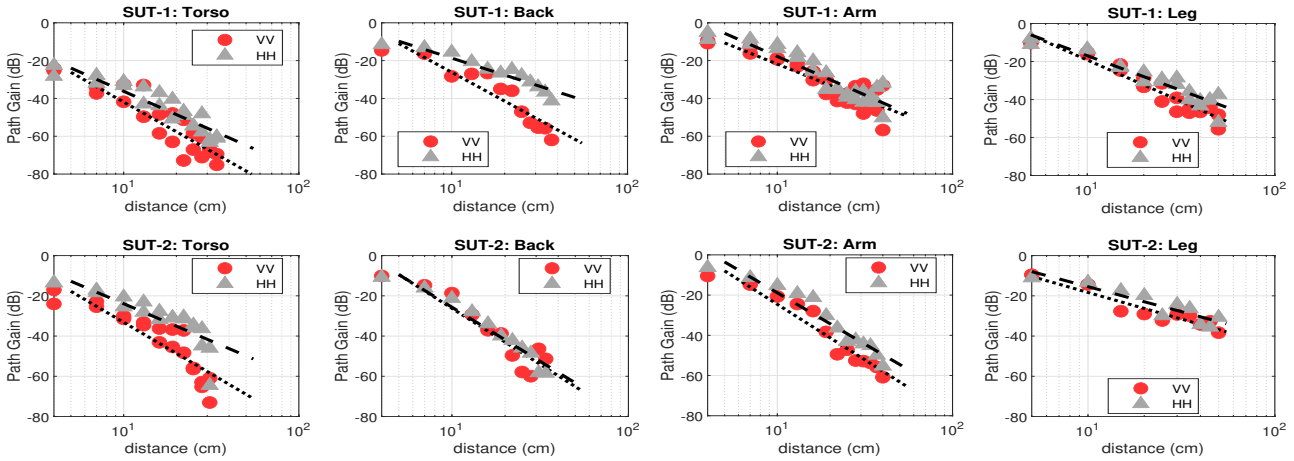


Fig. 4. Comparison of the modeled path gains for different polarizations of Tx-Rx antennas on body (VV vs. HH) for two subjects along the arm, leg, front and back of the torso at 60 GHz. Measurements-VV: circles; measurements-HH: triangles; fit-VV: dotted line; fit-HH= dashed line.

TABLE I
PARAMETERS OF CHANNEL GAIN MODEL PRESENTED IN EQUATION 2.

| f (GHz) | $G_d^*$ | SUT-1 | | | | | | | | SUT-2 | | | | | | | |
|---|---|---|---|---|---|---|---|---|---|---|---|---|---|---|---|---|---|
| | | Torso | | Back | | Arm | | Leg | | Torso | | Back | | Arm | | Leg | |
| | | VV | HH | VV | HH | VV | HH | VV | HH | VV | HH | VV | HH | VV | HH | VV | HH |
| 0.9 | $G_{d0}$ (dB) | -16 | -26.7 | -17.4 | -27.6 | -20.2 | -19.1 | -16 | -15 | -17.5 | -24.9 | -16.8 | -20.9 | -16.6 | 16.1 | -14.5 | -12.4 |
| | n (-) | 2.7 | 3.2 | 2.5 | 2.2 | 2.4 | 2.7 | 2.1 | 2.2 | 2.2 | 2.6 | 2.1 | 2.2 | 2.7 | 3.2 | 2.1 | 2.1 |
| | $\sigma$ (dB) | 2.1 | 4.2 | 1.4 | 1.9 | 1 | 3.7 | 1.2 | 1.3 | 1.9 | 5.3 | 0.9 | 2.4 | 0.6 | 2.9 | 1 | 1.5 |
| 55 | $G_{d0}$ (dB) | -38.9 | -35.4 | -25 | -18.1 | -21.7 | -17.3 | -18.8 | -15.4 | -32 | -23 | -24.7 | -24.8 | -24.2 | -18.5 | -17.6 | -15 |
| | n (-) | 5.7 | 4.3 | 5.1 | 3 | 3.6 | 4 | 4.2 | 3.7 | 5 | 3.7 | 5.4 | 5.3 | 5.3 | 5.1 | 2.6 | 2.6 |
| | $\sigma$ (dB) | 6.4 | 4.4 | 5.3 | 3.4 | 4.6 | 4.6 | 3.4 | 4.3 | 6.7 | 7.3 | 5.5 | 4.2 | 4.2 | 4.1 | 2.6 | 2.7 |
| 60 | $G_{d0}$ (dB) | -41.9 | -36.2 | -26.2 | -18.7 | -21.8 | -17.8 | -19.2 | -16.9 | -33.2 | -23.9 | -26.2 | -25.7 | -24.6 | -18.9 | -18.3 | -15.4 |
| | n (-) | 5.2 | 4.1 | 5.1 | 3 | 3.7 | 4.1 | 4.3 | 3.7 | 5.1 | 3.7 | 5.6 | 5.4 | 5.5 | 5.1 | 2.6 | 2.4 |
| | $\sigma$ (dB) | 6.3 | 4.6 | 5.7 | 2.9 | 5.4 | 4.8 | 3.8 | 3.6 | 6.9 | 6.2 | 5.9 | 3.7 | 4.3 | 4.2 | 2.8 | 3.2 |
| 65 | $G_{d0}$ (dB) | -44 | -37.2 | -27.2 | -20 | -22.2 | -18.3 | -19.6 | -18.1 | -35.3 | -25.9 | -27.3 | -27.7 | -25.2 | -19.4 | -19.3 | -15 |
| | n (-) | 5 | 4.2 | 5.1 | 3 | 3.6 | 4 | 4.3 | 3.1 | 5.3 | 4.1 | 5.8 | 5.5 | 5.7 | 5 | 2.8 | 2.7 |
| | $\sigma$ (dB) | 7 | 5.4 | 6.3 | 3.1 | 5.4 | 5 | 4.1 | 4.7 | 7.6 | 7.7 | 6.3 | 5.3 | 5.2 | 4.4 | 3 | 3.2 |

*$d_0 = 10\ cm$. $n$ and $\sigma$ are the path gain exponent and variance of shadow fading, respectively.

TABLE II
COMPARISON OF FITTED PARAMETERS TO THE CHANNEL GAIN MEASUREMENTS ON THE TORSO (LOS) AND THE PATH FROM FRONT TORSO TO BACK (LOS+NLOS) AT 900 MHZ.

| | SUT-1: Torso | | | | SUT-2: Torso | | | |
|---|---|---|---|---|---|---|---|---|
| | LOS | | LOS+NLOS | | LOS | | LOS+NLOS | |
| $G_d$ | VV | HH | VV | HH | VV | HH | VV | HH |
| $G^*_{d_0}$ | -17.0 | -25.0 | -25.0 | -28.0 | -20.0 | -27.0 | -27.0 | -29.0 |
| n (-) | 2.8 | 2.5 | 2.7 | 3.6 | 2.2 | 3.3 | 2.8 | 2.6 |
| $\sigma$ (dB) | 0.98 | 0.99 | 3.2 | 1.7 | 1.3 | 2.5 | 3.0 | 4.1 |

$^*d_0 = 10\ cm$; $n$: path gain exponent; $\sigma$: variance of shadow fading.

noise mean value of the PDP is considered to ensure that noise data are not processed as multipath. Third, $\tau_0$ and $\tau_{rms}$ are calculated [26]:

$$\tau_0 = \frac{\sum_k P(\tau_k)\tau_k}{\sum_k P(\tau_k)} \tag{6}$$

$$\tau_{rms} = \sqrt{\frac{\sum_k P(\tau_k)\tau_k^2}{\sum_k P(\tau_k)} - (\tau_0)^2} \tag{7}$$

with $P(\tau_k)$ and $\tau_k$ the power and delay of the $k$-th bin, respectively.

## IV. RESULTS

### A. Channel gain: 900 MHz Band

Figure 3 compares the modeled path gains based on the measurements for different polarizations of Tx-Rx antennas (i.e. V and H) on different body locations for two studied subjects at 900 MHz. Table I lists the parameters of channel gain model for both subjects. For different body locations of SUT-1, $G_{d0}$ is in the range of -15 dB to -27.6 dB while the channel gain exponent ($n$) is in the 2.1 to 3.2 range. For SUT-2, $G_{d0}$ and $n$ are in the range of -12.4 dB to -24.9 dB and 2.1 to 3.2, respectively. Except horizontally polarized antennas on the torso, SUT-2 with a lower body mass index (BMI) of 19.6 $kg/m^2$ has larger $G_{d0}$ values compared to SUT-1 with a BMI of 26.3 $kg/m^2$. This difference in $G_{d0}$ is in the range of 0.6 dB (back: VV) to 6.7 dB (back: HH). This is in line with the findings of [27] that demonstrated lower path gain values (up to 13 dB lower) for people with a higher BMI. In addition, except the arm, $n$ for SUT-2 is smaller than SUT-1. For the path measured from front torso to the back (NLOS), the path gain decreases by 3-8 dB for SUT-1 and by 2-7 dB for SUT-2 compared to when the path is measured on the front torso (LOS) of the same subjects. The parameters of the channel gain model for LOS and NLOS paths on the torso are compared in Table II. Additionally, $n$ increases for NLOS compared to LOS scenario.

For both subjects, the channel gain is lower for the HH polarizations of the antennas resulting in a lower $G_{d0}$. $G_{d0}$ is lower by a factor of 0.5 dB (SUT-2: arm) up to 10.7 dB (SUT-1: torso). We also find a higher $n$ for HH in comparison to VV, with absolute differences up to 0.5. Dominance of the vertical polarization at low frequencies (<6 GHz) has been reported in literature [8], [28], [29]. The reason is the more curved propagation surface of body for H-polarization compared to V, resulting in faster attenuation of waves and a higher diffraction for horizontal polarization [29].

The shadow fading is a zero-mean Gaussian distribution with standard deviation $\sigma$. The $\sigma$ values are in between 0.6 dB (arm: VV, SUT-2) and 5.3 dB (torso: HH, SUT-2). Torso has the largest $\sigma$ values. This is due to the fact that more paths were measured along the torso (4 paths) compared to other locations on the body.

### B. Channel gain: 60 GHz Band

Figure 4 shows the modeled channel gains from the measurements at different locations on both subjects for different polarizations of Tx-Rx at 60 GHz. The parameters of the model are also listed in Table I for 55, 60 and 65 GHz. For SUT-1, $G_{d0}$ is in the range of [-15.4 to -38.9 dB], [-16.9 to -41.9 dB] and [-18.1 to -44 dB] (for all ranges smallest: torso-VV and largest: leg-HH), at 55 GHz, 60 GHz and 65 GHz, respectively. Similarly, for SUT-2, the smallest $G_{d0}$ is for VV antennas on the torso and the largest $G_{d0}$ is for HH antennas on the leg. This ranges from [-15 to -32 dB], [-15.4 to -33.2 dB] and [-15 to -35.3 dB] at 55 GHz, 60 GHz and 65 GHz, respectively. SUT-2 with a smaller BMI has higher $G_{d0}$ values for all locations on body and the results are consistent in the 55-65 GHz range. Similar results have been reported in [27]. This difference between $G_{d0}$ values is higher for larger parts of the body due to their larger propagation surface. Therefore, the shape and dimensions of different body parts are the main determinant for the path gain.

For SUT-1 in the 55-65 GHz range, $n$ is between 3.6-5.7 and in the 3-4.3 range for VV and HH antenna configurations, respectively. For SUT-2, $n$ lies between 2.6 to 5.8 and 2.4 to 5.5, for VV and HH polarizations, respectively. A value of $n = 4$ is consistent with surface waves [17]. For both subjects (except arm: SUT-1), the values of $n$ for VV are larger than those of HH which is contrary to 900 MHz (see Section IV-A). This implies higher propagation loss of the waves for V polarization in the mm-wave band compared to H for which scattering from the body surface is the case [17], [30]. In order to demonstrate that HH configuration results in higher path gains than VV due to propagation effect rather than antenna characteristics, we repeated the measurements on front and back of Torso for SUB-1 (see III-A2) replacing the Rx with a end-fire Yagi-Uda antenna designed for WBAN applications [31]. Table III presents the measured channel gain parameters at 60 GHz on fornt and back of the torso for SUT-1.

According to Table III, V-polarizations of antennas on both front and back of the torso has lower path gains (6-9 dB difference) and higher $n$ (a difference up to 2) compared to H. This is an excellent agreement with the results obtained using horn antennas (see Table I). The lower path gains and higher $n$ for Yagi-Uda antenna is due to its lower gain (12 dBi) compared to the horn antenna with a gain of 16 dBi at 60 GHz. The lower gain of the Yagi-Uda antenna ideally

This article has been accepted for publication in a future issue of this journal, but has not been fully edited. Content may change prior to final publication. Citation information: DOI 10.1109/TAP.2020.3045498, IEEE Transactions on Antennas and Propagation



TABLE III
FITTED PARAMETERS TO THE CHANNEL GAIN MEASUREMENTS ON FRONT AND BACK OF THE TORSO FOR SUT-1 USING THE END-FIRE YAGI-UDA ANTENNA [31] AS RECEIVER AT 60 GHZ.

| $G_d$ | SUT-1: Front Torso | | SUT-1: Back Torso | |
|---|---|---|---|---|
| | VV | HH | VV | HH |
| $G^*_{d_0}$ | -37.8 | -28.9 | -34.9 | -28.9 |
| n (-) | 6.7 | 4.7 | 5.7 | 4.4 |
| $\sigma$ (dB) | 8.1 | 4.4 | 5.5 | 4.6 |

$^*d_0$ =10 cm; $n$: path gain exponent; $\sigma$: variance of shadow fading.

results in lower $G_{d0}$ values compared to the horn-horn scenario. However, the separation distance between the Yagi-Uda antenna and skin was different compared to the horn antenna. Hence, a higher $n$ was obtained. In [32], it was shown that unlike lower frequencies at which VV dominates HH, in the 60 GHz band, HH polarisation could be dominant when the antenna is very close to the propagation (body) surface. More specifically, an antenna height in the 3-20 mm range could result in stronger HH signals compared to VV [32]. In this case, combined contribution of direct, surface and reflected paths must be considered. The relative strength of the surface waves depends not only on the polarization, but also on the dielectric parameters. Furthermore, Chahat *et al.* [17], found that antenna efficiency is very sensitive for V polarization compared to H and decreases significantly with reducing the antenna-body separation. Kammersgaard *et al.* [33] showed that the ratio of vertically to horizontally polarized electric fields decreases with increasing the frequency from 2 GHz to 6 GHz. To the best of our knowledge, a literature gap exists explicitly demonstrating the frequency where dominant polarization changes from V to H.

The channel gain decreases with increasing the frequency in the 55-65 GHz range. This was expected as larger relative distances (on-body) had to be covered in comparison to the wavelength at higher frequencies which implies a lower channel gain [17]. The difference in channel gain for 55 GHz and 65 GHz are about 2 dB w.r.t. the path gain at 60 GHz. This is due to the smaller wavelength and higher losses at higher frequencies.

The shadow fading is a zero-mean Gaussian distribution with standard deviation $\sigma$. The $\sigma$ is between 2.6 dB (leg: VV, SUT-2 at 55 GHz) and 7.7 dB (torso: HH, SUT-2 at 65 GHz). Path gain measurements on multiple paths along the torso result in a larger variation on the path gain compared to the back, arm and leg. Increasing the frequency slightly increases $\sigma$.

### C. Wrist to arm channel gain: Influence of rotation at 60 GHz

The channel gain for both subjects as a function of the rotation of Tx around the wrist is shown in Fig. 5. The parameters of the channel gain model (eq. 5) are listed in Table IV. The loss per angle is in the range of 0.26-0.49 $dB/^\circ$ and 0.18-0.62 $dB/^\circ$ for SUT-1 and 2, respectively in the 55-65 GHz range. For both subjects, we found larger losses per degree ($\alpha_1$) for rotation angles $|\theta| < 90$ compared to the angles $|\theta| > 90$ (Fig. 2). This is in agreement with our

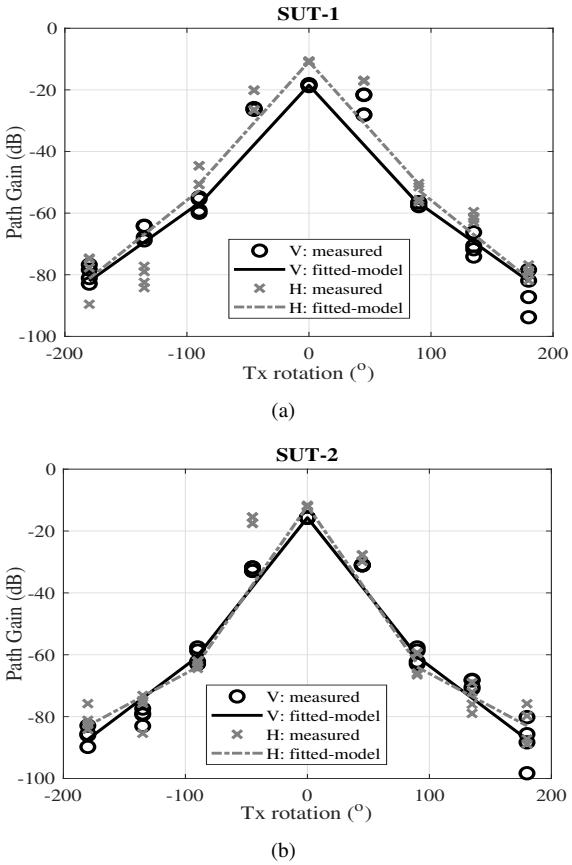


Fig. 5. Measurements of channel gain for rotation of the Tx around the arm at a distance of 10 cm from the Rx for the two subjects.

choice of the transition angle ($\theta_c = 90^\circ$). Similar results were found in [11] for propagation around human body in the 400-2400 MHz range. The losses for both polarizations are not significantly different for $|\theta| < 90$. For SUT-1, the losses per angle ($\alpha_2$) are higher for H-polarization while larger $\alpha_2$ is found for V-polarization on SUT-2. Most of the loss (on a logarithmic scale) occurred between rotation angles 45° and 90° as expected (see eq. 3). A better fit could be obtained by performing the measurements with more angular resolution and using a three-slope model. Additionally, we measured up to 53 dB loss over 90° rotation for both subjects. These higher losses for $|\theta| < 90$ indicate that 60 GHz-communications around the arm with a single antenna could be difficult especially for rotation angles $|\theta| > 90$. However, large losses measured over 90° rotation around the arm suggests a possibility for high signal-to-interference (SIR) ratio in 55-65 GHz range for channels that are 90° rotated towards each other on the arm (assuming similar path gains as Tx-Rx pair would rotate around the arm). For instance, using three or four antennas spaced 90° or 120° around the arm could provide a low-loss communication with high SIR ratio. It must be noted that the antennas used in this study have a narrow radiation pattern (3 dBm beamwidth of 14° to 24°) and a relatively high gain (16 dBi at 60 GHz).

This article has been accepted for publication in a future issue of this journal, but has not been fully edited. Content may change prior to final publication. Citation information: DOI 10.1109/TAP.2020.3045498, IEEE Transactions on Antennas and Propagation



TABLE IV
PARAMETERS OF THE CHANNEL GAIN MODEL IN EQ 5 FITTED TO THE MEASUREMENTS ON THE TWO STUDIED SUBJECTS.

| f (GHz) | Subject | $\alpha_1(dB/^\circ)$ V | $\alpha_1(dB/^\circ)$ H | $\alpha_2(dB/^\circ)$ V | $\alpha_2(dB/^\circ)$ H | $\sigma(dB)$ V | $\sigma(dB)$ H |
|---|---|---|---|---|---|---|---|
| 55 | SUT-1 | 0.39 | 0.45 | 0.29 | 0.34 | 1.7 | 2.2 |
| | SUT-2 | 0.47 | 0.54 | 0.27 | 0.21 | 2.2 | 1.9 |
| 60 | SUT-1 | 0.43 | 0.44 | 0.28 | 0.32 | 2.5 | 2.7 |
| | SUT-2 | 0.49 | 0.57 | 0.3 | 0.21 | 3.4 | 0.53 |
| 65 | SUT-1 | 0.45 | 0.49 | 0.26 | 0.3 | 2.8 | 4.4 |
| | SUT-2 | 0.53 | 0.62 | 0.19 | 0.18 | 4.3 | 5.7 |

### D. Delay spread

Figure 6(a) depicts the mean excess delay $\tau_0$ for HH antennas on both subjects in the 900 MHz band. Similar results were obtained for VV antennas. For both subjects (LOS) $\tau_0$ is between 2.66-5.17 ns and in the range of 2-6.3 ns for VV and HH configurations of antennas, respectively. This was expected since we measured larger path gains for VV compared to HH antennas in the 900 MHz band. Additionally, SUT-2 with a smaller BMI has slightly lower $\tau_0$ than SUT-1. This can be explained by the measurements in Section IV-A, where smaller BMI resulted in higher path gains (less absorption by the body) and consequently smaller delays. This is in agreement with findings of [27]. The value of $\tau_0$ for LOS measurements on different locations on both subjects increases by a factor 2.5 i.e. up to 12.6 ns (VV) and 14.6 ns (HH), when the path along torso is measured from front to back (NLOS) in the same band. The data follow a linear trend. Therefore, the measured $\tau_0$ values for each location on body are modeled using a linear least squares fitting as follows:

$$\tau_0(d) = A \times d + B \tag{8}$$

with $d$ the distance between Tx-Rx (cm), $A$ (ns/cm) and $B$ (ns) the parameters of the model. These parameters are listed in Table V. The value of $\tau_0$ increases up to a factor 0.05 ns per distance (cm) for LOS paths. For the NLOS path, a better fit is obtained by dividing the data to $d < 20\ cm$ and $d > 20\ cm$. For NLOS measurements on the torso, the slope of the fitted line (A′: $d > 20cm$) increases at least three times compared to LOS on the front torso. This is due to the multiple reflections of transmitted signals caused by the neck, shoulders and arms resulting in a larger delay. The fitted model for arm and leg are similar for both subjects and polarizations of Tx-Rx due to their similar dimensions w.r.t to the wavelength in the 900 MHz band.

The RMS delay spread ($\tau_{rms}$) at 900 MHz is in the range of 1.1-2.9 ns and 0.6-2.8 ns for VV- and HH-polarizations on both subjects, respectively. For the NLOS path along torso, $\tau_{rms}$ increases up to 8 ns. A linear fit similar to eq. (8), is used to model the data as a function of distance $d$ between Tx-Rx as $\tau_{rms}(d) = C \times d + D$ and $C$ (ns/cm) and $D$ (cm) are the parameters of the fit. These parameters are listed in Table V. For both polarizations, the fitted lines for leg and arm and the lines for front and back of the torso, have the lowest difference due to their comparable dimensions. For NLOS measurements, a breakpoint ($Bp$) of 20 cm was used

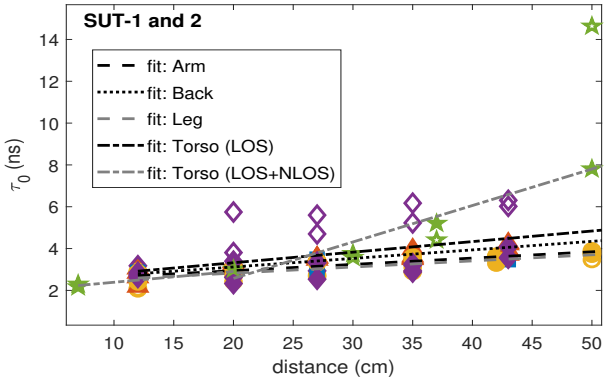


(a)

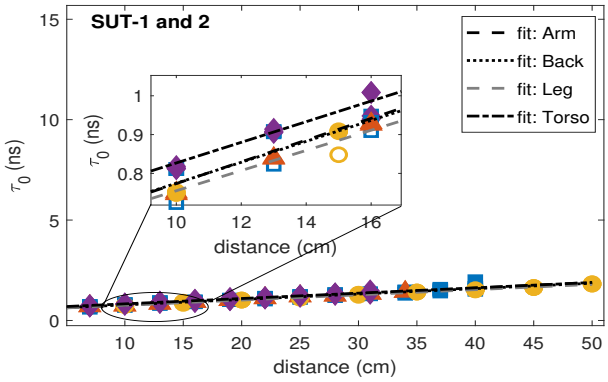


(b)

Fig. 6. Mean excess delay ($\tau_0$) measured (markers) for HH antennas on both subjects as a function of distance between Tx-Rx. (a) 900-MHz (b) 60 GHz. Measurements on SUT-1 and SUT-2 are indicated with empty and filled markers, respectively. Square: arm, Triangle: back, Circle: leg, Diamond: torso (LOS) and Pentagram: torso (LOS+NLOS).

to obtain a better fit. The value of $\tau_{rms}$ for both subjects and polarizations increases at least three times for the NLOS path on the torso compared to the LOS path at the same location. This indicates multiple reflections caused by the environment for NLOS scenario (torso) resulting is larger $\tau_{rms}$ values.

Figure 6(b) shows measured $\tau_0$ for HH antennas on both subjects at 60 GHz. The measured values for VV antennas are identical to those of HH. $\tau_0$ is in the 0.6-1.95 ns for both subjects and polarizations. This shows that the channel is not rich for 60 GHz (i.e. the multipath components are less, compared to microwave frequencies due to less reflections). The measurements perfectly follow a line that increases with increasing the distance between Tx and Rx. Therefore, the same model (eq. 8) is fitted to the measurements. The parameters of the fit ($A$ [ps/cm] and $B$ [ps]) are presented in Table V. Different fitted lines demonstrate a maximum slope of 3.5 ps/cm. At 60 GHz, the LOS component is dominant therefore, $\tau_0$ is less affected by the location of the path on body. In addition, even smallest parts like arm are relatively large compared to the wavelength at 60 GHz (5 mm).

The RMS delay spread at 60 GHz is between 0.021-0.67 ns and in the 0.022-0.6 ns range for VV- and HH-polarizations of the antennas on both subjects, respectively. $\tau_{rms}$ values for both subjects have no significant difference. This is due to the

This article has been accepted for publication in a future issue of this journal, but has not been fully edited. Content may change prior to final publication. Citation information: DOI 10.1109/TAP.2020.3045498, IEEE Transactions on Antennas and Propagation



TABLE V
PARAMETERS OF FITTED LINES TO THE MEASURED MEAN EXCESS DELAY AND RMS DELAY SPREAD.

| f (GHz) | Parameters | LOS | | LOS+NLOS | | | | LOS | | | |
|---|---|---|---|---|---|---|---|---|---|---|---|
| | | Torso | | Torso | | Back | | Arm | | Leg | |
| | | VV | HH | VV | HH | VV | HH | VV | HH | VV | HH |
| 0.9 | A (ns/cm) | 0.02 | 0.05 | 0.02 | 0.05 | 0.04 | 0.04 | 0.03 | 0.03 | 0.03 | 0.03 |
| | A′ (ns/cm) | - | - | 0.2 | 0.17 | - | - | - | - | - | - |
| | B (ns) | 3.2 | 2.3 | 2.4 | 1.9 | 2.9 | 2.3 | 2.8 | 2.3 | 2.8 | 2.2 |
| | B′ (ns) | - | - | -1 | -0.9 | - | - | - | - | - | - |
| | $\sigma_{\tau_0}$ (ns) | 0.34 | 1.1 | 0.14 | 0.1 | 0.26 | 0.23 | 0.34 | 0.2 | 0.38 | 0.28 |
| | $\sigma'_{\tau_0}$ (ns) | - | - | 1.6 | 2.6 | - | - | - | - | - | - |
| | C (ns/cm) | 0.02 | 0.03 | 0.02 | 0.03 | 0.03 | 0.03 | 0.01 | 0.01 | 0.01 | 0.01 |
| | C′ (ns/cm) | - | - | 0.18 | 0.09 | - | - | - | - | - | - |
| | D (ns) | 1.1 | 0.52 | 1.24 | 0.51 | 1 | 0.85 | 1.2 | 0.65 | 1.2 | 0.73 |
| | D′ (ns) | - | - | -2.1 | -0.03 | - | - | - | - | - | - |
| | $\sigma_{\tau_{rms}}$ (ns) | 0.25 | 0.43 | 0.05 | 0.01 | 0.32 | 0.29 | 0.13 | 0.11 | 0.26 | 0.09 |
| | $\sigma'_{\tau_{rms}}$ (ns) | - | - | 0.9 | 1.7 | - | - | - | - | - | - |
| 60 | A (ps/cm) | 28 | 27 | - | - | 26 | 27 | 27 | 28 | 26 | 26 |
| | B (ps) | 536 | 561 | - | - | 510 | 505 | 505 | 494 | 491 | 496 |
| | $\sigma_{\tau_0}$ (ps) | 21 | 52 | - | - | 14 | 16 | 31 | 68 | 24 | 20 |
| | C (ps/cm) | -0.46 | -0.12 | - | - | -0.18 | -0.87 | 2.82 | 2.1 | 3.5 | 2 |
| | D (ps) | 57 | 49.4 | - | - | 45 | 66 | 4.7 | 22.3 | -16 | 28 |
| | $\sigma_{\tau_{rms}}$ (ps) | 21.3 | 27.3 | - | - | 9.4 | 14.6 | 69.6 | 92.1 | 112 | 126 |

For each location and polarization the data of both subjects are considered.
A two-slope model is used for NLOS measurements. The parameters of the second fit are denoted as $A'$, $B'$, $C'$, $D'$ and $\sigma'$.

smaller wavelength at 60 GHz compared to the dimensions of the body. The presented results in Table I show larger $\sigma$ for the 60 GHz compared to 900 MHz. This means that the radiation into the body is less at 60 GHz due to the smaller penetration depth of the mm-waves into the body, which results in smaller delay values compared to lower frequencies (i.e. 900 MHz). Similar to the mean excess delay, a linear least squares fit is used to model data with $C$ (ps/cm) and $D$ (ns) parameters of the model. These parameters are listed in Table V.

### *E. Comparison: 900 MHz vs. 60 GHz*

*1) Comparison of path gain:* In the 900 MHz band, channel gains were measured in the range of -15 dB to -27.6 dB for both subjects. These values decrease to -15.4 dB to -44 dB for the 55-65 GHz range due to smaller wavelength and thus higher losses in body and/or higher reflections on the body surface. The path gain exponent ($n$) varies between 2.1-3.2 in the 900 MHz band and is in the range of 2.4-5.8 in the 60 GHz band. This indicates that at mm-wave frequencies the path gain drops quicker with increasing the distance between Tx and Rx.

In the 900 MHz band, V-polarization resulted in higher channel gains since horizontally polarized fields attenuate faster due to the curved propagation surface of the body. In contrast, in the 55-65 GHz range, higher path gains were measured for H-polarization of antennas. Firstly, absorption of vertically polarized E-fields is higher than that of horizontally polarized fields. Secondly, the antenna efficiency is significantly affected and decreases for V-polarized antennas reducing the antenna-body separation. This means that there are scenarios in which 60 GHz is the better choice over 900 MHz. Therefore, H polarization is desirable for antenna design for close distances for which extensions away from the body is not needed.

In both frequency bands, SUT-2 with a smaller BMI had higher path gain values. Increasing the frequency from 55 GHz to 65 GHz decreases the channel gain since the distances on body are relatively large compared to the wavelength. Note that our study is limited to two subjects, further investigations on more subjects (with different gender, BMI, etc.) constitute one of the perspectives of this study.

*2) Comparison of delay spread:* In the 900 MHz band, $\tau_0$ values are in the range of 2-6.3 ns for both subjects. These values increase up to 14.6 ns when the path is measured from front torso to back (NLOS) compared to LOS paths on the torso. $\tau_0$ is smaller for SUT-2 with a smaller BMI and smaller body measurements. The values of $\tau_{rms}$ are smaller than 3 ns for both subjects but it increases up to 8 ns for the NLOS path on the torso. Additionally, for both subjects the fitted models to the leg and arm and the fitted model to front and back of torso have high similarities, which correspond to their similar dimensions.

For both subjects in the 60 GHz band, $\tau_0$ values are smaller than 2 ns (factor 3 smaller than $\tau_0$ at 900 MHz) and the values for both polarizations of antennas are identical. This means that due to less reflections at 60 GHZ, the multipath components are less than 900 MHz. At 60 GHz LOS component is dominant, therefore, the delay spread is less affected by the location of the path on body. The values of $\tau_{rms}$ are smaller than 0.3 ns for both subjects and polarizations, which is 10 times smaller than $\tau_{rms}$ at 900 MHz. $\tau_{rms}$ increases with increasing the distance between the transmitter and the receiver as expected.

## V. CONCLUSIONS

In this paper, on-body propagation is experimentally characterized in the 900 MHz and 60 GHz bands for two vertical and horizontal polarizations. Different locations on body are considered including arm, leg, front and back of torso for two human male subjects. The channel parameters are extracted from measurements i.e. path gain and delay spread. We measured a minimum reference path gain of -27.6 dB and -44 dB in the 900 MHz and 60 GHz bands, respectively. Additionally, a path gain exponent $2 < n < 3$ is obtained for the 900 MHz band while in the 60 GHz band $2.4 < n < 6$. Vertical and horizontal polarizations resulted in higher path gains in the 900 MHz and 60 GHz bands, respectively. The results are in good agreement with literature. We also found

that the subject with a smaller body mass index (BMI) exhibits higher path gains compared to the subject with a larger BMI. For 60 GHz band, a wrist to arm scenario is studied with a transmitter antenna rotated 360° around the arm at a fixed distance from a receiver antenna. In this case, the loss per angle is up to 0.49 $dB/^\circ$ for both subjects. The losses for the H polarization of the antennas are higher than those of V for rotation angles smaller than 90 degrees. Most of the loss occurred between rotation angles of 45° and 90°. This suggests a possibility for high signal-to-interference (SIR) ratio in 55-65 GHz range for channels that are rotated 90° towards each other.

A mean excess delay up to 6.3 ns is obtained at 900 MHz while it decreases to <2 ns (3 times smaller) in the 60 GHz band. Additionally, a root-mean square (RMS) delay spread of 3 ns is obtained for the 900 MHz band. In the 60 GHz band, line-of-sight propagation is dominant, therefore, the RMS delay spread decrease to 0.3 ns, which is 10 times smaller compared to the 900 MHz band.

Based on our findings, H polarization at 60 GHz might be desirable for applications at short distances for which extensions away from the body are not needed. Smaller delays at 60 GHz cause less intersymbol interference and consequently, less transmit power is needed at 60 GHz compared to 900 MHz. However, the attenuation of mm-waves is higher than microwaves. To compensate for these losses, using higher gain antennas for shorter distances at 60 GHz could be a solution without need to increase the transmit power at 60 GHz. The preference of 60 GHz to 900 MHz, and vice versa, is case specific and thus there is not a unique general conclusion.

Future research includes statistical analysis of on-body wireless channels at higher frequencies, as well as demonstrating the frequency where dominant polarization changes from V to H. Additionally, the work presented in this paper will be extended to multiple subjects with different body morphologies (e.g., different gender, age, BMI, etc.).

## REFERENCES


[1] M. Chen, S. Gonzalez, A. Vasilakos, H. Cao, and V. C. Leung, "Body area networks: A survey," *Mobile networks and applications*, vol. 16, no. 2, pp. 171–193, 2011.

[2] M. Ghamari, B. Janko, R. Sherratt, W. Harwin, R. Piechockic, and C. Soltanpur, "A survey on wireless body area networks for ehealthcare systems in residential environments," *Sensors*, vol. 16, no. 6, p. 831, 2016.

[3] N. Katayama, K. Takizawa, T. Aoyagi, J.-i. Takada, H.-B. Li, and R. Kohno, "Channel model on various frequency bands for wearable body area network," *IEICE transactions on communications*, vol. 92, no. 2, pp. 418–424, 2009.

[4] L. Roelens, W. Joseph, E. Reusens, G. Vermeeren, and L. Martens, "Characterization of Scattering Parameters Near a Flat Phantom for Wireless Body Area Networks," *IEEE Trans. Electromagn. Compat.*, vol. 50, no. 1, pp. 185–193, Feb. 2008.

[5] A. Thielens, R. Benarrouch, S. Wielandt, M. Anderson, A. Moin, A. Cathelin, and J. Rabaey, "A comparative study of on-body radio-frequency links in the 420 MHz-2.4 GHz range," *Sensors*, vol. 18, no. 12, p. 4165, 2018.

[6] P. S. Hall, Y. I. Nechayev, C. C. Constantinou, Y. Hao, A. Alomainy, R. Dubrovka, and C. G. Parini, "Antennas and propagation for on-body communication systems," in *11th International Symposium on Antenna Technology and Applied Electromagnetics [ANTEM 2005]*. IEEE, 2005, pp. 1–7.

[7] J. Grosinger and M. Fischer, "Indoor on-body channel measurements at 900 MHz," in *2011 IEEE-APS Topical Conference on Antennas and Propagation in Wireless Communications*. IEEE, 2011, pp. 1037–1040.

[8] S. L. Cotton, R. D'Errico, and C. Oestges, "A review of radio channel models for body centric communications," *Radio Science*, vol. 49, no. 6, pp. 371–388, 2014.

[9] E. Reusens, W. Joseph, B. Latré, B. Braem, G. Vermeeren, E. Tanghe, L. Martens, I. Moerman, and C. Blondia, "Characterization of on-body communication channel and energy efficient topology design for wireless body area networks," *IEEE Trans. Inf. Technol. Biomed.*, vol. 13, no. 6, pp. 933–945, 2009.

[10] A. Fort, F. Keshmiri, G. R. Crusats, C. Craeye, and C. Oestges, "A body area propagation model derived from fundamental principles: Analytical analysis and comparison with measurements," *IEEE Trans. Antennas Propag.*, vol. 58, no. 2, pp. 503–514, 2009.

[11] J. Ryckaert, P. De Doncker, R. Meys, A. de Le Hoye, and S. Donnay, "Channel model for wireless communication around human body," *Electronics letters*, vol. 40, no. 9, pp. 543–544, 2004.

[12] A. Thielens, C. Baumbauer, M. G. Anderson, J. Ting, A. C. Arias, and J. M. Rabaey, "Feasability of on-body backscattering in the uhf-rfid band using screen-printed dipole antennas," in *2019 13th International Symposium on Medical Information and Communication Technology (ISMICT)*. IEEE, 2019, pp. 1–5.

[13] J. M. Rabaey, "The human intranet–where swarms and humans meet," *IEEE Pervasive Comput.*, vol. 14, no. 1, pp. 78–83, 2015.

[14] A. Pellegrini, A. Brizzi, L. Zhang, K. Ali, Y. Hao, X. Wu, C. Constantinou, Y. Nechayev, P. Hall, N. Chahat *et al.*, "Antennas and propagation for body-centric wireless communications at millimeter-wave frequencies: A review [wireless corner]," *IEEE Antennas Propag. Mag.*, vol. 55, no. 4, pp. 262–287, 2013.

[15] N. Chahat, M. Zhadobov, L. Le Coq, and R. Sauleau, "Wearable endfire textile antenna for on-body communications at 60 GHz," *IEEE Antennas Wireless Propag. Lett.*, vol. 11, pp. 799–802, 2012.

[16] N. Chahat, M. Zhadobov, S. A. Muhammad, L. Le Coq, and R. Sauleau, "60-GHz textile antenna array for body-centric communications," *IEEE Trans. Antennas Propag.*, vol. 61, no. 4, pp. 1816–1824, 2012.

[17] N. Chahat, G. Valerio, M. Zhadobov, and R. Sauleau, "On-body propagation at 60 GHz," *IEEE Trans. Antennas Propag.*, vol. 61, no. 4, pp. 1876–1888, 2013.

[18] P. Hall, Y. Hao, and S. Cotton, "Advances in antennas and propagation for body centric wireless communications," in *Proceedings of the Fourth European Conference on Antennas and Propagation*. IEEE, 2010, pp. 1–7.

[19] L. Petrillo, T. Mavridis, J. Sarrazin, J.-M. Dricot, A. Benlarbi-Delai, and P. De Doncker, "Ban working frequency: A trade-off between antenna efficiency and propagation losses," in *The 8th European Conference on Antennas and Propagation (EuCAP 2014)*. IEEE, 2014, pp. 3368–3369.

[20] K. Fujii, M. Takahashi, K. Ito, K. Hachisuka, Y. Terauchi, Y. Kishi, K. Sasaki, and K. Itao, "Study on the Transmission Mechanism for Wearable Device Using the Human Body as a Transmission Channel," *IEICE Transactions on Communications*, vol. E88-B, no. 6, pp. 2401–2410, Jun. 2005.

[21] J. Wang, Y. Nishikawa, and T. Shibata, "Analysis of On-Body Transmission Mechanism and Characteristic Based on an Electromagnetic Field Approach," *IEEE Trans. Microw. Theory Tech.*, vol. 57, no. 10, pp. 2464–2470, Oct. 2009.

[22] J. Bae, H. Cho, K. Song, H. Lee, and H.-J. Yoo, "The signal transmission mechanism on the surface of human body for body channel communication," *IEEE Trans. Microw. Theory Tech.*, vol. 60, no. 3, pp. 582–593, 2012.

[23] K. Norton, "The propagation of radio waves over the surface of the earth and in the upper atmosphere–part i," *Proceedings of the Institute of Radio Engineers*, vol. 24, no. 10, pp. 1367–1387, Oct. 1936.

[24] J. Park, H. Garudadri, and P. P. Mercier, "Channel modeling of miniaturized battery-powered capacitive human body communication systems," *IEEE Trans. Biomed. Eng.*, vol. 64, no. 2, pp. 452–462, 2017.

[25] C. A. Balanis, *Antenna theory: analysis and design*. Wiley-Interscience, 2005.

[26] T. Rappaport, *Wireless Communications: Principles and Practice*, 2nd ed. Upper Saddle River, NJ, USA: Prentice Hall PTR, 2001.

[27] S. Sangodoyin and A. F. Molisch, "Impact of Body Mass Index on Ultrawideband MIMO BAN Channels-Measurements and Statistical Model," *IEEE Trans. Wireless Commun.*, vol. 17, no. 9, pp. 6067–6081, Sep. 2018.

[28] T. Uusitupa and T. Aoyagi, "Analysis of dynamic on-body communication channels for various movements and polarization schemes at 2.45

ghz," *IEEE Trans. Antennas Propag.*, vol. 61, no. 12, pp. 6168–6179, Dec 2013.

[29] P. S. Hall, Y. Hao, Y. I. Nechayev, A. Alomainy, C. C. Constantinou, C. Parini, M. R. Kamarudin, T. Z. Salim, D. T. Hee, R. Dubrovka, A. S. Owadally, W. Song, A. Serra, P. Nepa, M. Gallo, and M. Bozzetti, "Antennas and propagation for on-body communication systems," *IEEE Antennas Propag. Mag.*, vol. 49, no. 3, pp. 41–58, Jun. 2007.

[30] M. Zhadobov, N. Chahat, R. Sauleau, C. Le Quement, and Y. Le Drean, "Millimeter-wave interactions with the human body: state of knowledge and recent advances," *Int J Microw Wirel Technol.*, vol. 3, no. 2, p. 237–247, 2011.

[31] N. Chahat, C. Leduc, M. Zhadobov, and R. Sauleau, "Antennas and interaction with the body for body-centric wireless communications at millimeter-waves," in *2013 7th European Conference on Antennas and Propagation (EuCAP)*, Apr. 2013, pp. 772–775.

[32] Y. I. Nechayev, C. C. Constantinou, X. Wu, and P. S. Hall, "De-Polarization of On-Body Channels and Polarization Diversity at 60 GHz," *IEEE Trans. Antennas Propag.*, vol. 62, no. 12, pp. 6519–6523, Dec. 2014.

[33] N. P. B. Kammersgaard, S. H. Kvist, J. Thaysen, and K. B. Jakobsen, "Electromagnetic fields at the surface of human-body cylinders," in *2016 International Workshop on Antenna Technology (iWAT)*, Feb. 2016, pp. 170–173.

**Reza Aminzadeh** received the M.Sc. degree in Electrical Engineering (Digital Electronics) from Sharif University of Technology, Iran, in 2014 and the Ph.D. degree in Electrical Engineering from Ghent University, Belgium, in 2020. In 2015, he joined the Waves group at the Department of Information Technology (INTEC), Ghent University, Belgium, as a Ph.D. student. His research was mainly focused on the design of wireless body area networks to characterize human exposure to radio-frequency electromagnetic fields. During November 2019, he was a visiting researcher at the Institute of Electronics and Telecommunications of Rennes (IETR), Rennes, France, where he focused on wearable personal exposimeters for the mm-wave band. Since January 2020, he is a postdoctoral researcher at Waves (UGent-imec). From 2012 to 2014, Reza Aminzadeh was a researcher at the Sharif University of Technology computational electromagnetics lab. His focus was on the numerical and experimental assessment of millimeter-wave reflectometry to detect skin cancer. Dr. Aminzadeh was served as a technical program committee member for the $14^{th}$, $15^{th}$, and $17^{th}$ National Iranian Student Conference on Electrical Engineering (ISCEE) during 2011-2014. He is the author or co-author of more than 30 peer-reviewed scientific journals and conference papers in bioelectromagnetics. Reza Aminzadeh is the recipient of the third Best Platform Presentation and Scientific Paper Award in BioEM2018, the Joint Meeting of The Bioelectromagnetics Society (BEMS) and the European Bioelectromagnetics Association (EBEA). His research interests include numerical and experimental dosimetry, wearable antenna design, on/in body radio wave propagation, measurement and theoretical modeling of biological tissues' dielectric properties, and development of tissue-equivalent phantoms for the mm-wave band, including the 5G technology.

**Arno Thielens** graduated in September 2010 from Ghent University as a master of science in engineering: applied physics. In the same year, he joined the Waves group, at that time known as WiCa, of Ghent University's information technology (INTEC) department as a PhD student. His research focused on personal exposure assessment to radio-frequency electromagnetic fields and numerical dosimetry. He obtained a PhD in Applied Physics at Ghent University in May 2015. Since June 2015, he is working as a post-doctoral researcher at Waves. He was a post-doctoral fellow of the IWT (Institute for Science and Innovation, Flanders, Belgium) from January 2016 up to May 2017. He obtained an FWO [PEGASUS]$^2$ Marie Skłodowska-Curie Fellowship in 2017 funded by the European Union's Horizon 2020 research and innovation programme under the Marie Skłodowska-Curie grant agreement No 665501 with the research Foundation Flanders (FWO). He also received an Honorary Fellowship by the Belgian American Education Foundation (BAEF) in the same year. In June 2017, he joined the Berkeley Wireless Research Center at the University of California, Berkeley, where he is working on the development of the human intranet. Dr. Thielens is the recipient of the Joseph James Morrissey Memorial Award issued by the Bioelectromagnetics Society (BEMS) and the European Bio Electromagnetics Association (EBEA) in June 2013. He also received the 2015 International Union of Radio Science (Union Radio-Scientifique Internationale or URSI) young scientist award.

**Maxim Zhadobov** (S'05–M'07–SM'15) received the M.S. degree in electromagnetics from the University of Nizhny Novgorod, Russia, in 2003, and the Ph.D. and Habilitation à Diriger des Recherches degrees from the IETR (Institut d'Electronique et des Technologies du numerique), University of Rennes 1, France, in 2006 and 2016, respectively. He was a Postdoctoral Researcher with the Center for Biomedical Physics, Temple University, Philadelphia, PA, USA, until 2008, and then joined the French National Center for Scientific Research (CNRS). He is currently the Principal Investigator in biomedical electromagnetics with the IETR/CNRS and head of the WAVES Team, IETR. His scientific interests and research activities are in the field of innovative biomedical applications of electromagnetic fields and associated technologies. He coauthored 5 book chapters, 5 patents, more than 75 research papers in peer-reviewed international journals and 180 contributions to conferences and workshops. His review article in the Int. J. Microwave Wireless Techn. has been the most cited paper in 2016-2020. A paper published by his research group in 2019 is in Journal Top 100 of Nature Scientific Reports. He has been involved in 23 research projects (12 as PI). Dr. Zhadobov was the TPC co-chair of BioEM 2021, Honolulu, Hawaii and BioEM 2020, Oxford, UK. He was a TPC member and / or session organizer at international conferences, including BioEM 2019, EuMW 2019, IEEE iWEM 2017, MobiHealth 2015-2017, BodyNets 2016, and IMWS-Bio 2014. He is an elected member of EBEA Council, senior member of IEEE, member of IEEE TC95.4, and vice-president of URSI France Commission K. He served as a guest editor of several special issues, including "Human Exposure in 5G and 6G Scenarios" of Applied Sciences and "Advanced Electromagnetic Biosensors for Medical, Environmental and Industrial Applications" of Sensors. He also served on review boards of more than 15 international journals and conferences, and has been acting as an expert at research councils worldwide. He received CNRS Medal in 2018, EBEA Award for Excellence in Bioelectromagnetics in 2015, and Brittany's Young Scientist Award in 2010. Since 2010, Ph.D. students he supervised received 7 national scientific awards and 5 awards from the Bioelectromagnetics Society, URSI and IEEE Antennas and Propagation Society.

**Luc Martens** (M'92) received the M.Sc. degree in electrical engineering from Ghent University, Ghent, Belgium, in 1986, and the Ph.D. degree, in 1990. From 1986 to 1990, he was a Research Assistant with the Department of Information Technology, Ghent University. During this period, his scientific research focused on the physical aspects of hyperthermic cancer therapy. His research dealt with electromagnetic and thermal modeling, and the development of measurement systems for that application. Since 1991, he has been managing the WAVES Research Group, INTEC. The WAVES Research Group is part of the imec Institute, since 2004. Since 1993, he has been a Professor with Ghent University. He has authored or co-authored more than 300 publications in the domain of electromagnetic channel predictions, dosimetry, exposure systems and health, and wireless communications. His research interests include modeling and measurement of electromagnetic channels, in electromagnetic exposure, e.g., around telecommunication networks and systems such as cellular base station antennas and in energy consumption of wireless networks.

**Wout Joseph** (M'05–SM'12) was born in Ostend, Belgium, in 1977. He received the M.Sc. and Ph.D. degrees in electrical engineering from Ghent University, Ghent, Belgium, in 2000 and 2005, respectively. From 2000 to 2005, he was a Research Assistant with the Department of Information Technology, Ghent University. During this period, his scientific research focused on electromagnetic exposure assessment. Since 2005, he has been a Postdoctoral Researcher with INTEC, UGent-imec. Since 2009, he has been a Professor in the domain of experimental characterization of wireless communication systems. His research interests include measuring and modeling electromagnetic fields around base stations for mobile communications, health effects of exposure to electromagnetic radiation, electromagnetic exposure assessment, propagation for wireless communication systems, and antennas and calibration. He is specialized in wireless performance analysis and quality of experience. From 2007 to 2013, he was a Postdoctoral Fellow of the FWO-V (Research Foundation-Flanders).